PCCP

Accepted Manuscript

This is an *Accepted Manuscript*, which has been through the Royal Society of Chemistry peer review process and has been accepted for publication.

Accepted Manuscripts are published online shortly after acceptance, before technical editing, formatting and proof reading. Using this free service, authors can make their results available to the community, in citable form, before we publish the edited article. We will replace this *Accepted Manuscript* with the edited and formatted *Advance Article* as soon as it is available.

You can find more information about *Accepted Manuscripts* in the Information for Authors.

Please note that technical editing may introduce minor changes to the text and/or graphics, which may alter content. The journal's standard Terms & Conditions and the Ethical guidelines still apply. In no event shall the Royal Society of Chemistry be held responsible for any errors or omissions in this *Accepted Manuscript* or any consequences arising from the use of any information it contains.

ROYAL SOCIETY OF CHEMISTRY

www.rsc.org/pccp

Mechanisms of Enhanced Sulfur Tolerance on Samarium (Sm)-doped Cerium Oxide (CeO_2) from First Principles

Dong-Hee Lim[1), 2)], Hee Su Kim[1)], Sung Pil Yoon[1)], Jonghee Han[1)], Chang Won Yoon[1)], Sun Hee Choi[1)]

Suk Woo Nam[1)], and Hyung Chul Ham[1),*]

[1)] Fuel Cell Research Center, Korea Institute of Science and Technology (KIST),

Hwarangno 14-gil 5, Seongbuk-gu, Seoul 136-791, Republic of Korea

[2)] Department of Environmental Engineering, Chungbuk National University

52 Naesudong-ro, Heungdeok-gu, Cheongju, Chungbuk 361-763, Republic of Korea

*Corresponding Author: Hyung Chul Ham

Email: hchahm@kist.re.kr

Phone: +82-2-958-5889, Fax: +82-2-958-5199

ABSTRACT

The role of samarium (Sm) 4*f* states and Sm-perturbed O 2*p* states in determining the sulfur tolerance of Sm-doped CeO_2 was elucidated by using the density functional theory (DFT)+U calculation. We find that the sulfur tolerance of Sm-doped CeO_2 is closely related to the modification of O 2*p* states by the strong interaction between Sm 4*f* and O 2*p* states. In particular, the availability of unoccupied O 2*p* states near the Fermi level is responsible for enhancing the sulfur tolerance of Sm-doped CeO_2 compared to the pure CeO_2 by increasing the activity of surface lattice oxygen toward sulfur adsorbate, by weakening the interaction between Sm–O, and by increasing the migration tendency of subsurface oxygen ion toward the surface.

TABLE OF CONTENTS

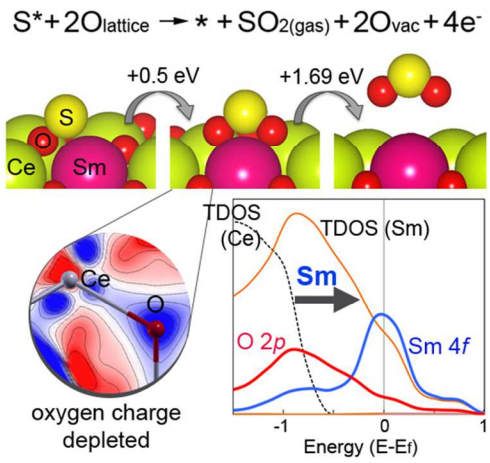

Keywords: Sulfur poisoning, solid oxide fuel cell, Samarium, CeO_2, *f* electron

Introduction

One of the main challenges in the development of anodes for solid oxide fuel cells (SOFCs) is the prevention of sulfur poisoning of Ni-based anodes because sulfur can block the active sites of the Ni anode and deteriorate the electrochemical performance of SOFCs.[1, 2] Recently, modifications of Ni-based anodes with ceria (CeO_2)-based materials has shown promise in reducing sulfur poisoning owing to the affinity of CeO_2 for sulfide at high temperature.[3-6] By coating ceria onto conventional nickel/yttria-stabilized zirconia (Ni/YSZ), improved SOFC cell performance was obtained[7, 8] because of the sulfur adsorption by ceria.

Furthermore, samarium (Sm) doping of CeO_2 may lead to enhanced sulfur tolerance and cell performance. Sm-doped ceria (SDC)-coated Ni/YSZ may serve as a more effective sulfur adsorbent than ceria, and has resulted in stable cell performance in the presence of 500 ppm of H_2S over 800 h.[9, 10] Approximately 25 to 50% improvement of the cell performance has been achieved with SDC-coated Ni/YSZ than with ceria-coated Ni/YSZ and conventional Ni/YSZ owing to the enhanced sulfur adsorbing capability of Sm and enlarged triple-phase boundary (electrode-electrolyte-gas phase) areas that reduce electrode polarization in the former.[9, 11, 12] The underlying mechanism governing the sulfur tolerance of Sm-doped CeO_2-based materials still remains unclear.

Recently, the origin of sulfur poisoning on Ni-based anode materials has been investigated using density functional theory (DFT). Zeng et al.[13] found that the smaller ionic radius of cation dopant X^{3+} results in the higher sulfur tolerance on Ni/XSZ (X_2O_3 stabilized zirconia), which is attributed to the fact that the dopant size directly influences the Ni−XSZ interaction and in turn affects the Ni−S interaction. Malyi et al.[14] revealed that the hybridization of Ni 3*d* and S 3*p* states serves an important role in the Ni−S interaction on Ni surfaces. Lu et al.[15] investigated the interaction of atomic sulfur with the ceria surfaces and found that sulfur tends to be in the CeO_2(111) after replacing oxygen, but on the CeO_2(110) surface as SO_2^{2-}. Mayernick et al.[16] examined H_2S adsorption and dissociation on Lanthanum (La)- and

Terbium (Tb)-doped CeO_2(111) by using DFT+U and ab initio thermodynamics, and indicated that sub-stoichiometric oxygen vacancies play an important role in sulfur adsorption process occurring via H_2S adsorption and dissociation where a strong endergonic molecular adsorption of H_2S is the rate limiting step.

In this study, we investigated the role of Sm in determining the sulfur tolerance of Sm-doped CeO_2 ($Sm_xCe_{1-x}O_2$) using spin-polarized DFT+U calculations. We examined the oxidation of H_2S on $Sm_xCe_{1-x}O_2$ and stoichiometric CeO_2 by calculating the reaction energetics and energy barriers of various reaction pathways. H_2S oxidation proceeds via H_2S decomposition ($H_2S^* \rightarrow HS^* + H^* \rightarrow S^* + H^* + H^*$) and SO_2 formation ($S^* + O^* + O^* \rightarrow SO^* + O^* \rightarrow SO_2^*$) (asterisk (*) denotes adsorbed species hereafter) as shown in Supporting Information, Figure S1. We also present the electronic properties of Sm-doped CeO_2 and stoichiometric CeO_2 to elucidate the origin of sulfur tolerance in CeO_2-based materials.

Computational Methodology

Spin-polarized DFT+U calculations were performed using the Vienna *ab-initio* Simulation Package (VASP)[17] within with the generalized gradient approximation (GGA-PBE[18]). The projector augmented wave (PAW) method with a planewave basis set was employed to describe the interaction between core and valence electrons[19, 20]. A plane-wave expansion with a kinetic energy cutoff of 400 eV was employed with a Gaussian smearing with a width of 0.2 eV. The integration of the Brillouin zone was conducted using a 4 × 4 × 1 Monkhorst-Pack grid[21] for the 2×2 CeO_2(111) slab model, where three Ce atom layers and six O atom layers are present as shown in Figure 1A (this nine layer slab model is be close to converged with respect to slab thickness and has been used in previous studies[22-24]).

The Sm-doped CeO_2 was modeled by introducing a Sm-doping atom to substitute Ce atoms in the CeO_2 (111) slab. Here a Sm dopant was located on the top surface, rather than on the subsurface since Sm dopant tends to segregate on the CeO_2 surface, rather than migrate into the bulk[25, 26].

The geometries were optimized until the forces were reduced below 0.05 eV/Å. A Hubbard-U term, U = 5 eV, was added to properly describe the localized nature of the 4f electrons of Ce.[27, 28] Furthermore, the climbing image-nudged elastic band (CI-NEB)[29] method was employed to calculate the activation energy for H_2S decomposition and SO_2 formation along the examined pathway.

The charge difference density ($\Delta n(\mathbf{r})$) plots were obtained by subtracting the charge densities of the separated adsorbate and the CeO_2 (or Sm-doped CeO_2) surface from the charge density of the adsorbate−surface system as follows:

$$\Delta n(\mathbf{r}) = n_{surf+adsorbate}(\mathbf{r}) - [\, n_{surf}(\mathbf{r}) + n_{adsorbate}(\mathbf{r}) \,] \tag{1}$$

where $n_{surf+adsorbate}(\mathbf{r})$, $n_{surf}(\mathbf{r})$, and $n_{adsorbate}(\mathbf{r})$ are the electron charge distributions of the surface with adsorbed species, isolated surface, and isolated adsorbate, respectively. The source of the isolated adsorbate and surface structures used for the charge difference density calculations have been directly obtained from the optimized structures of the bound systems, rather than the optimized free adsorbate and surface systems.

The oxygen vacancy formation energy per oxygen atom (E_{form}) is calculated as:

$$E_{form} = \left(E_{vac} - E_{perfect} + n(\tfrac{1}{2}E_{O_2})\right)/n \tag{2}$$

where E_{vac} and $E_{perfect}$ are the total energies of oxygen vacant and perfect surface, respectively. n is the number of oxygen vacancy and E_{O2} is the total energy of oxygen molecule.

The adsorption energy (E_{ads}) of an adsorbate is defined as $E_{ads} = E_{substrate+adsorbate} - E_{substrate} - E_{adsorbate}$, where $E_{substrate+adsorbate}$, $E_{substrate}$, and $E_{adsorbate}$ are the total energies of a substrate and adsorbate (e.g., CeO_2 with adsorbed sulfur), a substrate (e.g., CeO_2), and a gas phase adsorbate (e.g., sulfur). A

negative adsorption energy indicates that adsorption is exothermic (stable) with respect to the free gas-phase adsorbate.

Results and Discussion

The modified electronic properties of Sm-doped CeO_2 were examined by analyzing the charge density difference caused by the replacement of Ce by Sm (See Figure 1). Because of the higher electron density of Sm ([Xe]$4f^6 6s^2$) than that of Ce ([Xe]$4f^1 5d^1 6s^2$), strong charge accumulation is observed at the location of Sm (up to 3.60 e/Å^3) in the charge density difference plot. Importantly, the electron charge of the neighboring lattice oxygen atoms of Sm becomes depleted because of the replacement of Ce^{4+} by Sm^{3+}, resulting in a relatively weak interaction of lattice oxygen with the Sm-doped CeO_2 surface. The weaker Ce−O interaction on Sm-doped CeO_2 is supported by the oxygen vacancy formation energy as shown in Table 1. Less energy is required to create one or two oxygen vacancies in Sm-doped CeO_2 compared to that required for stoichiometric CeO_2. This observation may imply that the lattice oxygen with depleted electron charge helps promote sulfur oxidation by lowering the activation energy for SO_2 formation ($S^* \rightarrow SO_2^*$). In the ensuing discussion, we demonstrate the enhanced SO_2 formation by analyzing the reaction pathways and estimating the activation energies using the CI-NEB[29] method.

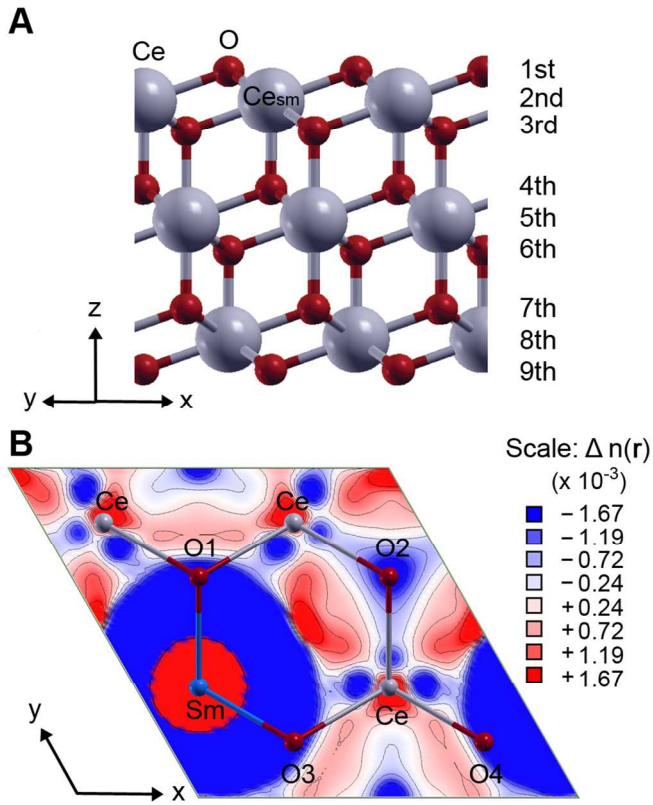

Figure 1. (A) Side view of the 2×2 CeO_2 structure consisting of three Ce and four O layers. (B) Charge density difference ($\Delta n(\mathbf{r})$ in units of $e/Å^3$) of Sm-doped CeO_2 upon Sm replacement defined by $[n(\mathbf{r})_{\text{Sm-doped } CeO_2} - n(\mathbf{r})_{CeO_2}]$, where $n(\mathbf{r})_{\text{Sm-doped } CeO_2}$ and $n(\mathbf{r})_{CeO_2}$ are the charge densities of Sm-doped CeO_2 and stoichiometric CeO_2 surfaces. Ce_{sm} indicates the Ce atom replaced by Sm in (B).

Table 1. Oxygen vacancy formation energies depending on the number of oxygen vacancies. Superscripts *a*, *b*, *c*, *d*, and *e* indicate oxygen vacancy locations of (O1), (O2), (O1, O2), (O1, O4), and (O1, O3), respectively, as depicted in Figure 1B.

	One vacancy (eV/O atom)	Two vacancies (eV/O atom)
CeO_2	3.33^a	$3.01^{c,d}$
Sm-doped CeO_2	1.79^a, 1.97^b	2.65^c, 2.32^e

Prior to detailed examination of the reaction pathways and corresponding activation energy, an overall reaction pathway from H_2S adsorption to SO_2 desorption was examined as shown in the

Supporting Information, Figure S2, indicating that the H_2S decomposition reaction is exothermic whereas the SO_2 desorption reaction is endothermic. The reaction limiting step of the sulfur removal mechanism may lie in the last step of SO_2 desorption. In-depth understanding of the effect of Sm on the reaction pathways can be achieved by comparing the activation energies required for each reaction step on both surfaces.

Figure 2 shows the lowest-energy reaction pathways of H_2S decomposition on stoichiometric CeO_2 and Sm-doped CeO_2, demonstrating that Sm doping promotes H_2S decomposition by lowering the activation energy required for each step. Sm doping significantly lowers the activation energy barrier of the $HS^* + H^* \rightarrow S^* + H^* + H^*$ step from 0.64 to 0.12 eV, and furthermore, turns an endothermic reaction into an exothermic one at the last step of H_2S decomposition. The H_2S molecule binds weakly on the top site of Ce or Sm where the sulfur is bound on Ce or Sm with respective adsorption energies of −0.21 and −0.22 eV for stoichiometric CeO_2 and Sm-doped CeO_2, which agrees with previous DFT[30, 31] and experimental[32] studies. Notably, the adsorption configuration of $S^* + H^* + H^*$ on CeO_2, where sulfur is located at the top site of Ce, is ~0.15–0.19 eV more stable than those in which sulfur is located on the bridge or hollow sites of Ce (Supporting Information, Figure S3); the most stable configuration of $S^* + H^* + H^*$ is where sulfur interacts directly with lattice oxygen (Figure 2A). Marrocchelli and Yildiz[30] also showed that the $HS^* + H^* \rightarrow S^* + H^* + H^*$ reaction on stoichiometric $CeO_2(111)$ is exothermic when atomic sulfur is bound to the lattice oxygen, and an energy barrier of 0.69 eV is present between the two steps, which may be attributed to an intermediate step where sulfur is bound to the top site of Ce as shown here.

The CeO_2 and Sm-doped CeO_2 surfaces differ notably in terms of the stabilization of atomic sulfur and hydrogen on each surface; Sm doping considerably enhances the stability of the $S^* + H^* + H^*$ step. This result agrees well with the empirical observation that Sm doping enhances the sulfur-adsorbent properties of CeO_2 in recent SOFC studies employing a $Ce_{0.8}Sm_{0.2}O_2$-coated Ni/YSZ anode.[9, 10] In the presence of 100 ppm of H_2S, the polarization resistance of the $Ce_{0.8}Sm_{0.2}O_2$-coated Ni/YSZ

anode (40%) increased to a lesser extent than that of the CeO_2-coated Ni/YSZ anode (90%);[9] this demonstrates that Sm enhances the capture of sulfur by CeO_2, where it is stored as Ce_2O_2S.[9] The current DFT results also demonstrate that Sm-doped CeO_2 can better decompose the H_2S molecule into atomic sulfur compared to stoichiometric CeO_2, which may lead to a higher storage of Ce_2O_2S on Sm-doped CeO_2 than on stoichiometric CeO_2.

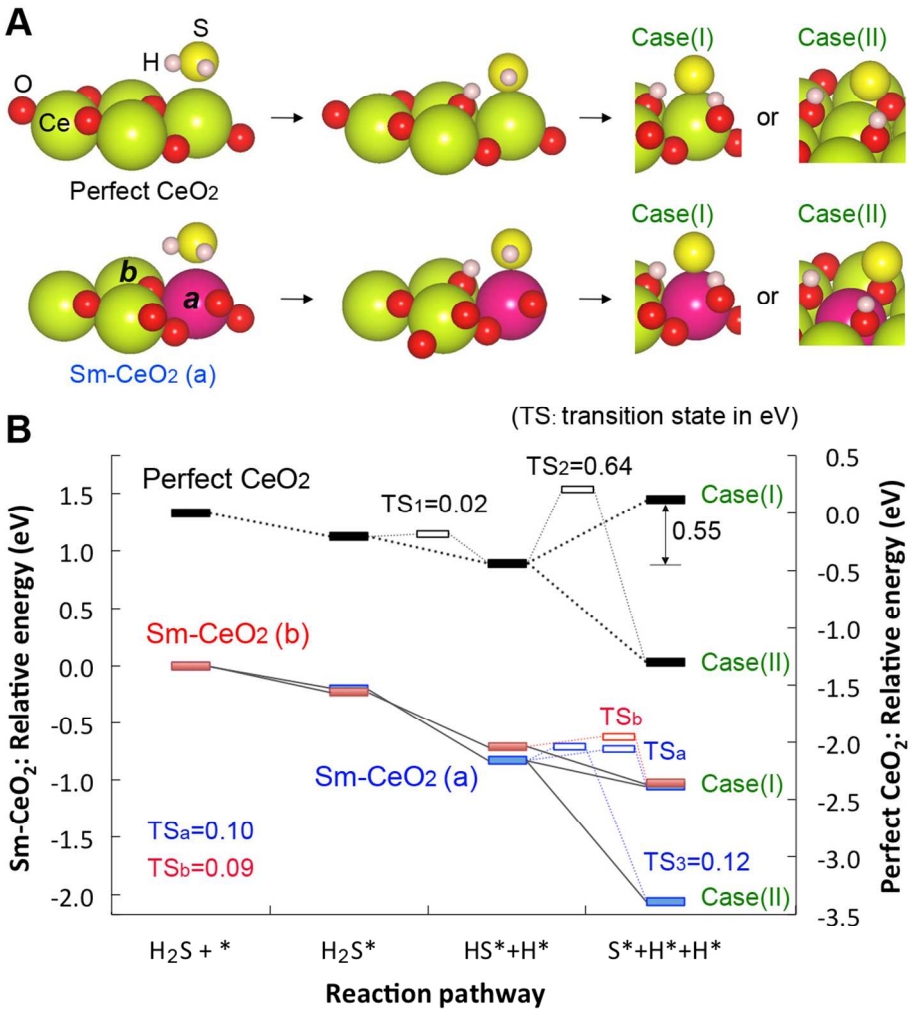

Figure 2. The lowest-energy reaction pathways (A) and relative energy diagrams (B) of H_2S decomposition on stoichiometric CeO_2 (dashed lines) and Sm-doped CeO_2 (solid lines). *a* and *b* indicate the location of Sm depending on Sm-doped CeO_2 (a) and (b), respectively. Empty rectangles represent transition states (TS) in eV. The absence of TS between two steps indicates the absence of an energy

barrier. Case(I) and Case(II) represent the $S^* + H^* + H^*$ configurations where sulfur is located on the top of Ce and lattice oxygen, respectively.

The enhanced decomposition of H_2S on Sm-doped CeO_2 may be attributed to the modified electronic structure of Sm-doped CeO_2 due to Sm doping. Figure 3A shows a comparison of the total density of states (DOS) between stoichiometric CeO_2 and Sm-doped CeO_2. For the stoichiometric CeO_2 case, we find that a gap is present between the top of the O 2*p* valence band and the bottom of the unoccupied Ce 4*f* conduction band, which agrees well with previous DFT studies.[27, 33, 34] On the other hand, for the Sm-doped CeO_2 case, our calculation predicts that a new gap state between the O 2*p*−Ce 4*f* gap is formed near the Fermi level. This new gap state is related to Sm 4*f* and Sm-perturbed O 2*p* states, which may be responsible for the significantly increased stability of sulfur radicals and in turn enhanced H_2S decomposition on Sm-doped CeO_2 compared to that on stoichiometric CeO_2.

To unravel the relative role of Sm 4*f* and Sm-perturbed O 2*p* states in determining the surface reactivity toward the sulfur species, we calculated the sulfur adsorption energy at various surface sites and projected density of state (PDOS) onto Sm 4*f* and O 2*p* states. First, our calculation shows the slight enhancement of the sulfur adsorption energy (E_{ad}) at the Sm top site [E_{ad} = −0.88eV] on Sm-doped CeO_2, compared to the Ce top site on stoichiometric CeO_2 [E_{ad} = −0.70eV]. On the other hand, we find a significant improvement of the sulfur adsorption energy at the O top site on Sm-doped CeO_2 by 0.82eV in comparison with stoichiometric CeO_2 case, indicating that the surface O site is the critical factor to boost the sulfur stability in Sm-doped CeO_2 (Supporting Information, Table S1). Figure 4 shows the charge difference density upon sulfur adsorption on lattice oxygen in Sm-doped CeO_2 and stoichiometric CeO_2 cases. We find the larger electronic charge accumulation in the bonding region between S 2*p* an O 2*p* orbital in Sm-doped CeO_2 than that in stoichiometric CeO_2 cases, suggesting the formation of much stronger covalent bond in Sm-doped CeO_2.

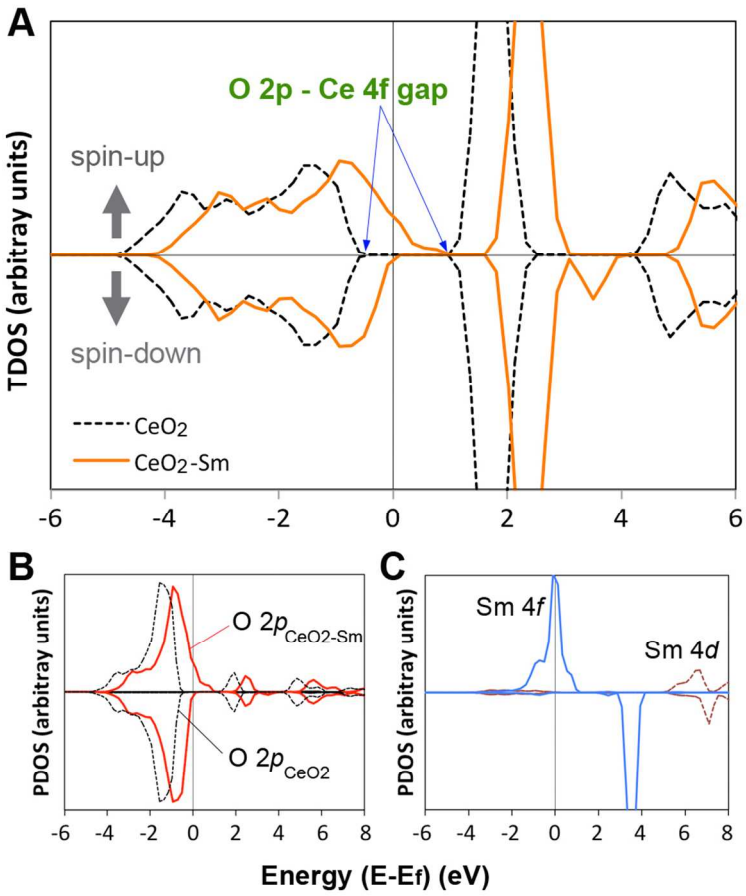

Figure 3. (A) Total density of states (TDOS) of stoichiometric CeO_2 (dashed lines) and Sm-doped CeO_2 (solid lines). (B) Projected density of states (PDOS) of surface oxygen 2*p* state (four O atoms) of stoichiometric CeO_2 and Sm-doped CeO_2. (C) PDOS of Sm 4*d* and 4*f* states. Spin-up and -down are indicated by positive and negative values, respectively. The Fermi energy is referenced at 0 eV.

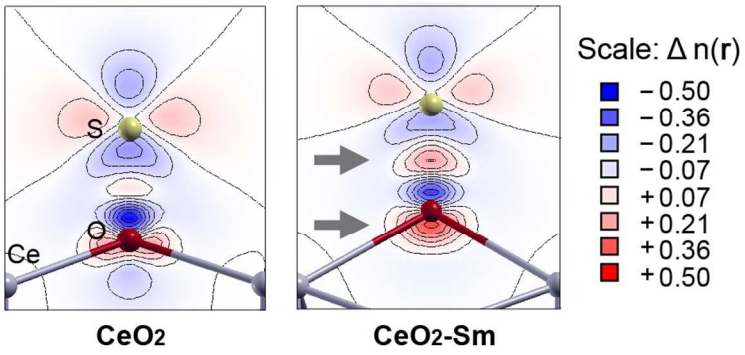

Figure 4. Charge difference density ($\Delta n(\mathbf{r})$ in units of e/Å^3) of stoichiometric CeO_2 and Sm-doped CeO_2 upon sulfur adsorption on lattice oxygen. Two arrows indicate strong charge depletion upon sulfur adsorption.

The dramatic enhancement of the surface activity at the lattice O site is related to the formation of unoccupied O 2*p* states caused by the strong mixing between Sm 4*f* and O 2*p* states. According to our DFT+U calculation on the PDOS of Sm 4*f* and O 2*p* states (Figure 3B and 3C), a significant overlap between Sm 4*f* and O 2*p* states are observed in the -1.7 eV $< E-E_f <$ 1.0 eV, suggesting a strong hybridization of Sm 4*f*–O 2*p* states in Sm-doped CeO_2. Notice no overlap between Ce 4*f*–O 2*p* states in stoichiometric CeO_2. Correspondingly, the PDOS of occupied O 2*p* states in Sm-doped CeO_2 noticeably shifts toward the Fermi level compared to the stoichiometric CeO_2 case. In particular, the onset of low binding energy tail shifts above the Fermi level, which results in the formation of unoccupied O 2*p* states in the 0 eV $< E-E_f <$ 1.0 eV. The different oxidation state of dopants and Bader charge analysis also support the creation of empty unoccupied O 2*p* states. Our DFT+U calculation shows that the oxidation state of Sm dopant is about +3 in Sm-doped CeO_2, which is lower than that of Ce atom (Ce^{4+}) (Note that the magnetization of Sm 4*f* states in Sm-doped CeO_2 is ~ 4.9*e*. Together with the fact that there is no electron in Sm 6*s* state, this indicates that the oxidation state of Sm is close to +3 in Sm-doped CeO_2). As a result, the electronic charge of O^{2-} perturbed by Sm 4*f* states is substantially decreased by 0.060*e* (from Bader charge analysis) compared to the O^{2-} case in stoichiometric CeO_2, leading to the formation of empty O 2*p* states.

Moreover, the unoccupied O 2*p* states above the Fermi level may weaken the binding energy between Sm and the lattice oxygen due to reduced electron density of oxygen, promoting the formation of oxygen vacancies (see comparison of oxygen vacancy formation energies in Table 1). A similar phenomenon has been reported for copper adsorbed-CeO_2(111) where the formation of oxygen

vacancies was promoted by formation of unoccupied states near the Fermi level upon copper adsorption.[27]

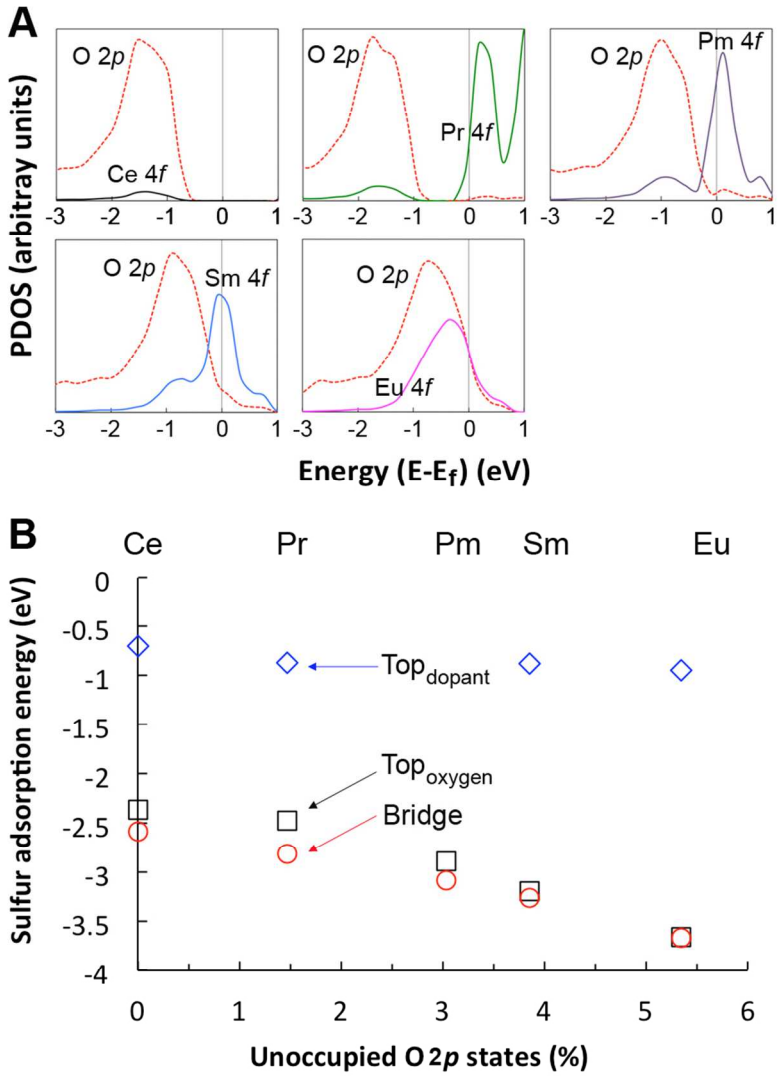

Figure 5. (A) PDOS of surface oxygen 2*p* (four O atoms) and dopant (Ce, Pr, Pm, Sm, and Eu) 4*f* (one dopant atom) states where spin-up and -down states are summed. The Fermi energy is referenced at 0 eV. (B) Sulfur adsorption energies on top sites of dopants (rhombus), top sites of surface lattice oxygen (square), and bridge sites of dopant-oxygen (circles). *x*-axis represents the portion of unoccupied lattice oxygen 2*p* states below 1 eV in PDOS. Sulfur on the top of dopants is restrained in *x* and *y* directions.

To better understand the importance of unoccupied O 2*p* states in determining the activity of surface lattice oxygen, the Sm atom in Sm-doped CeO_2 was replaced with three 4*f* shell dopants (i.e., praseodymium (Pr) ([Xe]$4f^3 6s^2$), promethium (Pm) ([Xe]$4f^5 6s^2$), and europium (Eu) ([Xe]$4f^7 6s^2$)), and the sulfur adsorption and the electronic properties of Pr-, Pm-, and Eu-doped CeO_2 were examined.

From the PDOS of O 2*p* states and dopant 4*f* states (See Figure 5A), we find that the number of unoccupied O 2*p* states strongly depends on the degree of overlap between O 2*p* states and dopant 4*f* states. That is, as the number of 4*f* electrons of dopants (Ce = 2, Pr = 3, Pm = 5, Sm = 6, and Eu = 7) increase, the hybridization of Sm 4*f*–O 2*p* states becomes stronger, leading to the increase of the number of unoccupied O 2*p* states of 4*f* shell dopant-perturbed oxygen ion (Ce = 0, Pr = 1.47, Pm = 3.04, Sm = 3.85, and Eu = 5.34 % in terms of the percentage of unoccupied O 2*p* state). TDOS and PDOS of Pr-, Pm-, Sm-, and Eu-doped CeO_2 are compared in Supporting Information, Figure S4.

In Figure 5B, the sulfur adsorption energy is displayed as a function of the number of unoccupied O 2*p* states. We find the improvement of sulfur adsorption energy at the O-associated surface sites (dopant-oxygen bridge sites) as the number of unoccupied O 2*p* states increases [Ce (−2.58) < Pr (−2.81) < Pm (−3.08) < Sm (−3.26) < Eu (−3.67 eV)]. This trend is inversely proportional to the oxygen vacancy formation energy depending on the 4*f* shell dopants (Ce (3.33) > Pr (2.96) > Pm (2.11) > Sm (1.79) > Eu (1.17 eV)), which is attributed to the increased depletion of electron density from oxygen as the shift of O 2*p* states above the Fermi level. This demonstrates that the availability of unoccupied O 2*p* states plays a key role in enhancing the stability of sulfur and in turn H_2S decomposition on the surface.

Figure 6 represents the lowest-energy reaction pathways of gas phase SO_2 production from adsorbed sulfur on stoichiometric CeO_2 and Sm-doped CeO_2. In this reaction scheme, adsorbed sulfur uses surface lattice oxygen to form SO^* and SO_2^* according to the following hypothesis, where adsorbed sulfur (S^*) is electrochemically oxidized by lattice oxygen that is replenished from oxygen ion flux from a cathode.[35-38]

$$S^{*} + 2O_{SDC} \rightarrow * + SO_{2(gas)} + 2V\ddot{o} + 4e^{-} \quad (1)$$

Here, O_{SDC}, *, and *Vö* represent a lattice oxygen, the SDC surface, and an oxygen vacancy in SDC, respectively. Although the H_2S reactions on ceria involve the formation of $H_2O_{(gas)}$ and $H_{2(gas)}$, a DFT calculation model based on Eq. (1) may provide enough insight into the role of Sm in determining the sulfur tolerance of SDC given that the resistance to sulfur poisoning is mainly attributed to the SO_2 desorption reaction.[35-37]

Our calculation predicts that Sm doping enhances the adsorbed SO_2 formation by lowering the activation energy for the $SO^{*} \rightarrow SO_2^{*} + V\ddot{o}$ step from 0.90 to 0.62 or 0.50, depending on the location of Sm (Figure 6B). The lowered energy barriers are related to the significant reduction of oxygen vacancy formation energy due to the weakened interaction between lattice oxygen and Sm dopant by the substantial existence of unoccupied O 2*p* states. Note that the oxygen vacancy formation energy is reduced by 1.54 (or 1.36) eV on Sm-doped CeO_2 compared to pure ceria as shown in Table 1.

The energy for the desorption of SO_2 on stoichiometric $CeO_2(111)$ is 2.05 eV, which agrees with the results of a previous DFT study in which the desorption energy was calculated at 1.96 eV. However, Sm doping lowers the desorption energy of SO_2 to 2.00 and 1.69 eV. The relatively more stabilized oxygen vacant Sm-doped CeO_2 surface compared to the oxygen vacant CeO_2 surface also contributes to enhancing sulfur removal by promoting SO_2 desorption. Notably, the significantly lowered SO_2 desorption energy of 1.69 eV on Sm-doped CeO_2 is due to the fact that the subsurface oxygen ion near Sm tends to migrate onto the surface during the SO_2 desorption. The calculated distances of migrated subsurface oxygen ions toward the surface in stoichiometric CeO_2 and Sm-doped CeO_2 are 0.35 and 1.07 Å, respectively (See Supporting Information, Figure S5), which implies that Sm doping may promote the migration process of oxygen ion formed at the subsurface toward the surface during the

SO_2 desorption, resulting in the further stabilization of oxygen vacant Sm-doped CeO_2 surface compared to stoichiometric CeO_2 and in turn the improvement of SO_2^* desorption energetics. This is also confirmed by higher exothermicity by 0.18 eV on Sm-doped CeO_2 than on stoichiometric CeO_2 for the complete migration process of oxygen ion from subsurface to surface.

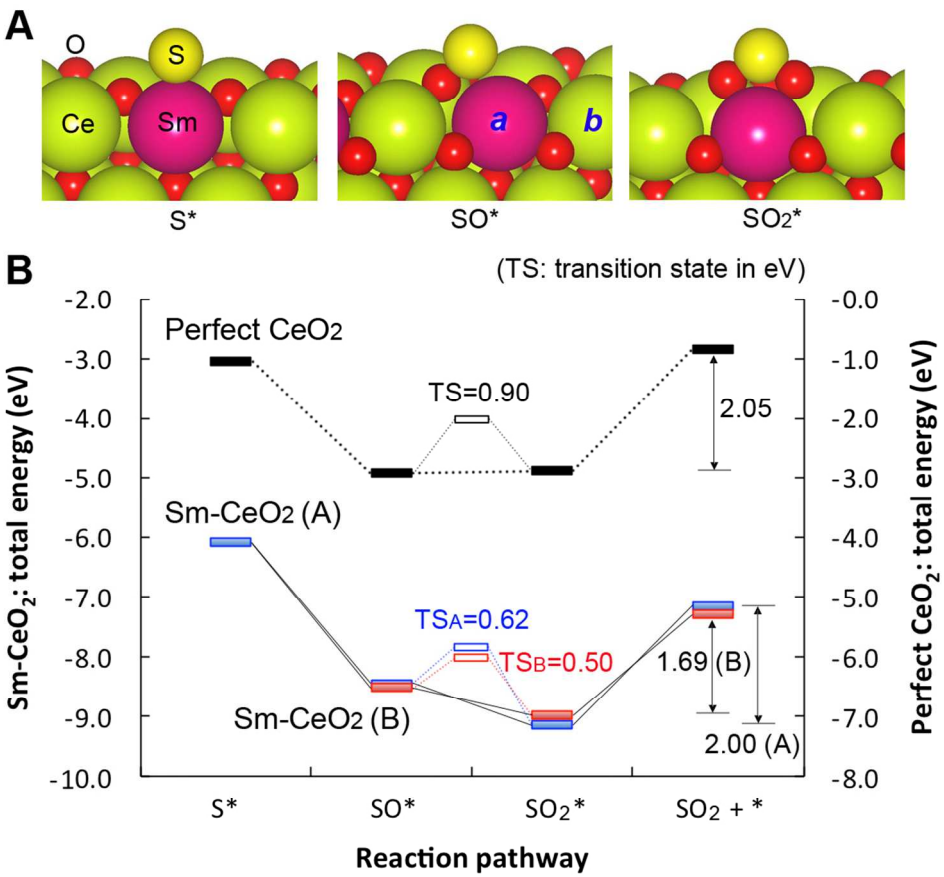

Figure 6. The lowest-energy reaction pathways (A) and energy diagrams (B) for SO_2 formation on stoichiometric CeO_2 (dashed lines) and Sm-doped CeO_2 (solid lines). *a* and *b* indicate the location of Sm depending on Sm-doped CeO_2 (A) and (B), respectively. Empty rectangles represent transition states (TS) in eV. The absence of TS between two steps indicates the absence of an energy barrier.

Conclusions

In summary, we find that the strong interaction between Sm 4*f* and O 2*p* states on Sm-doped CeO_2 increases the availability of unoccupied O 2*p* states near the Fermi level. The increased

unoccupied O 2*p* states in turn enhance the sulfur tolerance of Sm-doped CeO_2 compared to the pure ceria by boosting the stability of sulfur species in H_2S decomposition owing to the increased activity of surface lattice oxygen toward sulfur adsorption, by reducing the oxygen vacancy formation energy in SO_2 production due to the weakened interaction between Sm and O, and by further stabilizing the oxygen vacant surface in SO_2 desorption process attributed to the increased migration tendency of subsurface oxygen ion toward the surface. This work also hints on the importance of properly engineering the activity of oxygen ion in CeO_2-based materials by adding dopant.

Supporting Information

Schematic diagrams of H_2S decomposition and SO_2 formation pathways, adsorption energies of H_2S, HS, and S species, additional adsorption configurations of $S^* + H^* + H^*$ on $CeO_2(111)$, TDOS and PDOS of Pr-, Pm-, Sm-, and Eu-doped CeO_2, and configurations of diffused subsurface oxygen atoms. This materials is available free of charge via the Internet at http://pubs.acs.org.

Corresponding Author

*E-mail: hchahm@kist.re.kr. Phone: +82-2-958-5889, Fax: +82-2-958-5199

Acknowledgement

The current work was financially supported by the Global Research Laboratory (GRL) Program funded by the Ministry of Education, Science and Technology of Korea, and also supported by Basic Science Research Program through the National Research Foundation (NRF) of Korea funded by the Ministry of Education, Science and Technology (2012R1A6A3A04040490). The computational resources were supported by the Supercomputing Center/Korea Institute of Science and Technology Information with supercomputing resources including technical support (KSC-2013-C3-017).

References

1. Matsuzaki, Y.; Yasuda, I., The poisoning effect of sulfur-containing impurity gas on a SOFC anode: Part I. Dependence on temperature, time, and impurity concentration. *Solid State Ionics* **2000,** *132*, (3-4), 261-269.
2. Zha, S. W.; Cheng, Z.; Liu, M. L., Sulfur poisoning and regeneration of Ni-based anodes in solid oxide fuel cells. *Journal of the Electrochemical Society* **2007,** *154*, (2), B201-B206.
3. Li, Z. J.; Flytzani-Stephanopoulos, M., Cu-Cr-O and Cu-Ce-O regenerable oxide sorbents for hot gas desulfurization. *Industrial & Engineering Chemistry Research* **1997,** *36*, (1), 187-196.
4. Zeng, Y.; Zhang, S.; Groves, F. R.; Harrison, D. P., High temperature gas desulfurization with elemental sulfur production. *Chemical Engineering Science* **1999,** *54*, (15-16), 3007-3017.
5. Wang, Z.; Flytzani-Stephanopoulos, M., Cerium oxide-based sorbents for regenerative hot reformate gas desulfurization. *Energy & Fuels* **2005,** *19*, (5), 2089-2097.
6. Yi, K. B.; Podlaha, E. J.; Harrison, D. P., Ceria-zirconia high-temperature desulfurization sorbents. *Industrial & Engineering Chemistry Research* **2005,** *44*, (18), 7086-7091.
7. Kurokawa, H.; Sholklapper, T. Z.; Jacobson, C. P.; De Jonghe, L. C.; Visco, S. J., Ceria nanocoating for sulfur tolerant Ni-based anodes of solid oxide fuel cells. *Electrochemical and Solid State Letters* **2007,** *10*, (9), B135-B138.
8. Devianto, H.; Yoon, S. P.; Nam, S. W.; Han, J.; Lim, T.-H., The effect of a ceria coating on the H2S tolerance of a molten carbonate fuel cell. *Journal of Power Sources* **2006,** *159*, (2), 1147-1152.
9. Yun, J. W.; Yoon, S. P.; Park, S.; Kim, H. S.; Nam, S. W., Analysis of the regenerative H2S poisoning mechanism in Ce0.8Sm0.2O2-coated Ni/YSZ anodes for intermediate temperature solid oxide fuel cells. *International Journal of Hydrogen Energy* **2011,** *36*, (1), 787-796.
10. Yun, J. W.; Ham, H. C.; Kim, H. S.; Song, S. A.; Nam, S. W.; Yoon, S. P., Effects of the Sm0.2Ce0.8O2-delta Modification of a Ni-Based Anode on the H2S Tolerance for Intermediate Temperature Solid Oxide Fuel Cells. *Journal of the Electrochemical Society* **2013,** *160*, (2), F153-F161.
11. Yun, J. W.; Yoon, S. P.; Park, S.; Han, J.; Nam, S. W.; Lim, T.-H.; Kim, J.-S., Modifying the cathodes of intermediate-temperature solid oxide fuel cells with a Ce0.8Sm0.2O2 sol-gel coating. *International Journal of Hydrogen Energy* **2009,** *34*, (22), 9213-9219.
12. Yoon, S. P.; Han, J.; Nam, S. W.; Lim, T. H.; Hong, S. A., Improvement of anode performance by surface modification for solid oxide fuel cell running on hydrocarbon fuel. *Journal of Power Sources* **2004,** *136*, (1), 30-36.
13. Zeng, Z.; Bjorketun, M. E.; Ebbesen, S.; Mogensen, M. B.; Rossmeisl, J., Origin of electrolyte-dopant dependent sulfur poisoning of SOFC anodes. *Physical Chemistry Chemical Physics* **2013,** *15*, (18), 6769-6772.
14. Malyi, O. I.; Chen, Z.; Kulish, V. V.; Bai, K.; Wu, P., Density functional theory study of the effects of alloying additions on sulfur adsorption on nickel surfaces. *Applied Surface Science* **2013,** *264*, 320-328.
15. Lu, Z.; Kullgren, J.; Yang, Z.; Hermansson, K., Sulfidation of Ceria Surfaces from Sulfur and Sulfur Diffusion. *The Journal of Physical Chemistry C* **2012,** *116*, (15), 8417-8425.
16. Mayernick, A. D.; Li, R.; Dooley, K. M.; Janik, M. J., Energetics and Mechanism for H2S Adsorption by Ceria-Lanthanide Mixed Oxides: Implications for the Desulfurization of Biomass Gasifier Effluents. *The Journal of Physical Chemistry C* **2011,** *115*, (49), 24178-24188.
17. Kresse, G.; Furthmüller, J., Efficient iterative schemes for ab initio total-energy calculations using a plane-wave basis set. *Phys Rev B* **1996,** *54*, (16), 11169-11186.
18. Perdew, J. P.; Burke, K.; Ernzerhof, M., Generalized Gradient Approximation Made Simple. *Physical Review Letters* **1996,** *77*, (18), 3865-3868.
19. Blöchl, P. E., Projector augmented-wave method. *Phys Rev B* **1994,** *50*, (24), 17953-17979.
20. Kresse, G.; Joubert, D., From ultrasoft pseudopotentials to the projector augmented-wave method. *Phys Rev B* **1999,** *59*, (3), 1758-1775.
21. Monkhorst, H. J.; Pack, J. D., Special points for Brillouin-zone integrations. *Phys Rev B* **1976,** *13*, (12), 5188-5192.
22. Skorodumova, N. V.; Baudin, M.; Hermansson, K., Surface properties of CeO2 from first principles. *Phys Rev B* **2004,** *69*, (7).
23. Fabris, S.; Vicario, G.; Balducci, G.; de Gironcoli, S.; Baroni, S., Electronic and atomistic structures of clean and reduced ceria surfaces. *J Phys Chem B* **2005,** *109*, (48), 22860-22867.
24. Chafi, Z.; Keghouche, N.; Minot, C., DFT study of Ni-CeO2 interaction: Adsorption and insertion. *Surf Sci* **2007,** *601*, (11), 2323-2329.

25. Guo, M.; Lu, J. Q.; Wu, Y. N.; Wang, Y. J.; Luo, M. F., UV and Visible Raman Studies of Oxygen Vacancies in Rare-Earth-Doped Ceria. *Langmuir* **2011,** *27*, (7), 3872-3877.
26. Ismail, A.; Giorgi, J. B.; Woo, T. K., On the Atomistic Interactions That Direct Ion Conductivity and Defect Segregation in the Bulk and Surface of Samarium-Doped Ceria: A Genetic Algorithm Study. *J Phys Chem C* **2012,** *116*, (1), 704-713.
27. Yang, Z. X.; He, B. L.; Lu, Z. S.; Hermansson, K., Physisorbed, Chemisorbed, and Oxidized CO on Highly Active Cu-CeO2(111). *Journal of Physical Chemistry C* **2010,** *114*, (10), 4486-4494.
28. Kim, H. Y.; Henkelman, G., CO Oxidation at the Interface between Doped CeO2 and Supported Au Nanoclusters. *Journal of Physical Chemistry Letters* **2012,** *3*, (16), 2194-2199.
29. Henkelman, G.; Uberuaga, B. P.; Jonsson, H., A climbing image nudged elastic band method for finding saddle points and minimum energy paths. *Journal of Chemical Physics* **2000,** *113*, (22), 9901-9904.
30. Marrocchelli, D.; Yildiz, B., First-Principles Assessment of H2S and H2O Reaction Mechanisms and the Subsequent Hydrogen Absorption on the CeO2(111) Surface. *Journal of Physical Chemistry C* **2012,** *116*, (3), 2411-2424.
31. Chen, H.-T.; Choi, Y.; Liu, M.; Lin, M. C., A First-Principles Analysis for Sulfur Tolerance of CeO_2 in Solid Oxide Fuel Cells. *Journal of Physical Chemistry C* **2007,** *111*, (29), 11117-11122.
32. Mullins, D. R.; McDonald, T. S., Adsorption and reaction of hydrogen sulfide on thin-film cerium oxide. *Surface Science* **2007,** *601*, (21), 4931-4938.
33. Szabova, L.; Skala, T.; Matolinova, I.; Fabris, S.; Camellone, M. F.; Matolin, V., Copper-ceria interaction: A combined photoemission and DFT study. *Applied Surface Science* **2013,** *267*, 12-16.
34. Zhang, C.; Michaelides, A.; King, D. A.; Jenkins, S. J., *Oxygen vacancy clusters on ceria: Decisive role of cerium f electrons*. 2009; Vol. 79, p 075433.
35. Zha, S.; Cheng, Z.; Liu, M., Sulfur poisoning and regeneration of Ni-based anodes in solid oxide fuel cells. *Journal of the Electrochemical Society* **2007,** *154*, (2), B201-B206.
36. Cheng, Z.; Wang, J. H.; Choi, Y. M.; Yang, L.; Lin, M. C.; Liu, M. L., From Ni-YSZ to sulfur-tolerant anode materials for SOFCs: electrochemical behavior, in situ characterization, modeling, and future perspectives. *Energy & Environmental Science* **2011,** *4*, (11), 4380-4409.
37. Cheng, Z.; Zha, S. W.; Liu, M. L., Influence of cell voltage and current on sulfur poisoning behavior of solid oxide fuel cells. *Journal of Power Sources* **2007,** *172*, (2), 688-693.
38. Sasaki, K.; Susuki, K.; Iyoshi, A.; Uchimura, M.; Imamura, N.; Kusaba, H.; Teraoka, Y.; Fuchino, H.; Tsujimoto, K.; Uchida, Y.; Jingo, N., H2S poisoning of solid oxide fuel cells. *Journal of the Electrochemical Society* **2006,** *153*, (11), A2023-A2029.